Confinement effects in a guided-wave atom interferometer with millimeter-scale arm separation

J. H. T. Burke, B. Deissler, K. J. Hughes, and C. A. Sackett*
Department of Physics, University of Virginia, Charlottesville, Virginia 22904, USA
(Received 26 May 2008; published 14 August 2008)

Guided-wave atom interferometers measure interference effects using atoms held in a confining potential. In one common implementation, the confinement is primarily two dimensional, and the atoms move along the nearly free dimension after being manipulated by an off-resonant standing wave laser beam. In this configuration, residual confinement along the nominally free axis can introduce a phase gradient to the atoms that limits the arm separation of the interferometer. We experimentally investigate this effect in detail, and show that it can be alleviated by having the atoms undergo a more symmetric motion in the guide. This can be achieved by either using additional laser pulses or by allowing the atoms to freely oscillate in the potential. With these techniques, we demonstrate interferometer measurement times up to 72 ms and arm separations up to 0.42 mm with a well controlled phase, or times of 0.91 s and separations of 1.7 mm with an uncontrolled phase.

DOI: 10.1103/PhysRevA.78.023619 PACS number(s): 03.75.Dg, 37.25.+k

I. INTRODUCTION

Atom interferometry is a striking example of the particle-wave duality inherent in quantum mechanics. Beyond this, however, it has proven to be a practical and useful technique for several types of precision measurements [1]. Traditional atom interferometers use atoms moving freely through space, with only occasional manipulation by external fields to control their trajectory. With the development of laser cooling techniques and Bose-Einstein condensation, however, it has become possible to implement "guided-wave" atom interferometers, in which an applied potential directs the atomic motion at all times [2–9]. The advantages of guided-wave atom interferometry include the abilities to incorporate more complex trajectories and to support the atoms against gravity over long measurement periods. It is hoped that these advantages will eventually allow guided-wave interferometers to exceed the capabilities of free-space devices. Guided-wave atom interferometry presents several challenges, however, since it is critical that the guiding fields impart no uncontrolled quantum phase to the wave packets.

One limitation that is particularly important for interferometers using larger arm separation is the effect of longitudinal variations in the guiding potential. In several experiments to date [4,6,7], the "guide" is really an elongated harmonic trap, with atomic wave packets moving along the weak axis of the trap. The nonuniform potential imparts a spatially varying phase shift to the packets, so that different parts of the packet interfere with different phases and the overall visibility of the interference is degraded. In this paper, we explore this phenomenon in detail and present three results. First, we experimentally measure the phase gradients imposed on the atoms and confirm their relation to the visibility. Second, we demonstrate that the phase gradients can be greatly reduced by using a more symmetric trajectory for the atomic packets. We achieve packet separations of up to 0.42 mm in this way. Finally, by using an interferometer scheme in which the atoms freely oscillate in the confining potential, interference is still observed for separations of 1.7 mm. In the last case, however, environmental noise effects cause the phase to fluctuate randomly from one measurement to the next.

In order to explain these results, we briefly summarize our methods. Our interferometer has been described previously in Refs. [6,10], and the basic operation is illustrated in Fig. 1. To start, a Bose-Einstein condensate of 3×10^4 ^{87}Rb atoms is prepared in the $F=2, m_F=2$ hyperfine state and held in a time-orbiting potential waveguide with harmonic confinement at frequencies $(\omega_x,\omega_y,\omega_z)\approx 2\pi\times(6.0,1.1,3.3)$ Hz. This confinement is deliberately weak, making the atomic density and thus interaction effects small.

The atoms are manipulated using an off-resonant laser. The beam is reflected to form a standing wave aligned to the weak (y) axis of the waveguide. By applying two short pulses of this standing wave [11], atoms at rest in the $|0\rangle$ momentum state can be driven to a superposition of states moving with momentum $p=\pm 2\hbar k$: $|0\rangle\rightarrow(|2\hbar k\rangle+|-2\hbar k\rangle)/\sqrt{2}$, where k is the wave number of the standing wave laser. In our case, the packet speed $2\hbar k/m\equiv v_0$

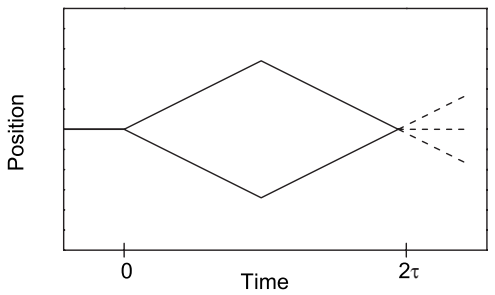

FIG. 1. Packet trajectories for the single-sided interferometer configuration. At time $t=0$, a Bose-Einstein condensate is split into two wave packets that move apart with velocities $\pm v_0$. At time τ the packets are reflected, and at time 2τ they are recombined. The resulting state depends on the phase difference between the paths. In actuality, the trajectories will be distorted by the weak harmonic potential in which the packets move.

*sackett@virginia.edu

=11.7 mm/s. As described in Ref. [12], this operation can be made very precise.

After this splitting is complete, the packets propagate away from each other in the y direction for a time τ. The standing wave is then applied a second time, with intensity and duration such that the reflection transition $|2\hbar k\rangle \leftrightarrow |-2\hbar k\rangle$ is driven. After a total time 2τ, the packets return to their initial position. For a single-sided interferometer as in Fig. 1, a third laser pulse, identical to the first splitting pulse, is then applied. If there is no phase difference between the two packets of atoms, this final pulse reverses the action of the first and all the atoms come back to rest. However, if a phase θ develops between the packets, some portion of the atoms will continue in the moving states. The fraction of atoms ending in the rest state, N_0/N, is given by $\cos^2(\theta/2)$. In practice, we control the phase θ by adjusting the position of the standing wave relative to the atoms before the final pulse [6].

In this geometry, it is easy to see how the axial confinement can produce a phase gradient across the packets. The packets have a length along the guide of L, set by the size of the initial condensate. As the packets move apart, the leading edge of the packet experiences a larger potential energy than the trailing edge, since it is further from the bottom of the potential. The leading edge therefore develops a larger phase, which continues to accumulate through the entire trajectory. Since the leading edge of one packet interferes with the trailing edge of the other, the phase difference between the packets has a spatial gradient.

A phase gradient also arises from atomic interactions. Due to the mean-field effect, atoms in one packet experience a repulsive potential proportional to the density of the other packet. As the two packets separate, the leading edges stop interacting before the trailing edges, causing a spatially varying phase. This effect is similar to that from the potential described above, but has the opposite sign since here the trailing edge acquires the larger phase.

Both of these problems were first recognized by Olshanii and Dunjko [13], who used them to explain the limited interferometer performance observed by Wang *et al.* [4]. Horikoshi and Nakagawa [7] demonstrated an interferometer using a similar geometry and showed that it, too, was limited to an arm separation consistent with that imposed by the phase gradient effect. In these experiments, the gradients were large enough that the packets could not be well-separated before the visibility was reduced to nearly zero. Olshanii *et al.* [13] and later Stickney *et al.* [14] suggested strategies to extend the arm separation by making the interaction and confinement effects cancel.

In our experiment, however, the two arms of the interferometer become well separated in space. In general, the interaction gradient cannot be a dominating effect in such a case, since the interaction gradient stops growing once the packets stop overlapping. So if the interaction gradient is sufficiently small to avoid washing out the visibility at the point where the packets separate, the effect will remain small thereafter. In contrast, the gradient from the confining potential will continue to grow, and therefore can become an important limitation. Because interferometers that grant individual access to their arms are potentially useful, an understanding of this regime is particularly important, and is the primary subject of our investigation.

To correct this problem, a more symmetric trajectory can be used. If the packets are not recombined at time 2τ, but instead pass through each other and follow a matching trajectory on the other side of the potential minimum, then the leading and trailing edges of the packet will switch roles. The gradient built up during the first one-half of the trajectory will cancel in the second one-half, restoring the visibility and extending the useful interaction time. We originally demonstrated an interferometer of this sort some time ago [6], but we here investigate specifically the gradient cancellation effect.

We discuss the theory and results for the single-sided interferometer in Sec. II, and find that it is indeed limited to small packet separations. In Sec. III we consider the more symmetric double-sided interferometer geometry, and show that the phase gradient is greatly reduced. Even then, however, the trajectories are not perfectly symmetric due to the action of the reflection pulses, and in Sec. IV we demonstrate that if the atoms are allowed to simply complete a full oscillation in the harmonic potential of the guide, interference can be observed at even much longer times. Section V offers a summary and conclusions.

II. SINGLE-SIDED INTERFEROMETER

We begin with a theoretical model of the interferometer operation. The atomic wave packets can be represented by mean-field wave functions ψ_1 and ψ_2 which satisfy the nonlinear Schrödinger equations

$$\left(-\frac{\hbar^2}{2m}\frac{\partial\psi_i}{\partial t} + V(y) + g[|\psi_i(y)|^2 + 2|\psi_j(y)|^2]\right)\psi_i = i\hbar\frac{\partial\psi_i}{\partial t} \tag{1}$$

for $i=1,2$ and $j\neq i$. Here $V(y)=(m\omega^2 y^2)/2$ is the confining potential and g characterizes the mean-field interactions. This description neglects fluctuation effects such as phase diffusion, which are expected to be small for our experimental parameters. We also approximate the system as one dimensional, since the condensate is extended along the weak axis of the trap and it is the phase gradient along that direction that affects the interference.

Immediately after the splitting pulse, the packets have a distribution corresponding to the initial condensate density n_0, given in the Thomas-Fermi limit as

$$n_0(y) = \begin{cases} \dfrac{\mu}{g}\left(1-\dfrac{y^2}{L^2}\right) & \text{if } V(y)<\mu, \\ 0 & \text{if } V(y)>\mu \end{cases} \tag{2}$$

for initial chemical potential μ and length $L=(2\mu)/(m\omega^2)$. In our experiment, $\mu \approx 2\pi\hbar \times 15$ Hz and $L\approx 55$ μm. After splitting, the packets are no longer in equilibrium, so as the experiment proceeds, the wave functions will evolve in a complicated way that is computationally intensive to model.

As a simple approximation, the internal dynamics can be neglected entirely and the packets treated as rigid bodies.

This approach is justified if the duration of the interferometer measurement is short compared to the periods of the relevant internal modes of the packets. It was used in Refs. [9,13] and we adopt it here as well. Stickney *et al.* introduced a less restrictive approximation allowing for quadratic phase variations across the packet, corresponding to linear expansion or contraction of the size. As seen below, we find the rigid-packet approximation to be adequate for the single-sided interferometer.

The centers of the two packets are denoted by $Y_1(t)$ and $Y_2(t)$. We define y_1 and y_2 as the positions relative to the packet centers, so that $Y_i+y_i=y$ for $i=1,2$. In the rigid-packet approximation, the phase acquired by packet i at position y_i can be expressed as

$$\phi_i(y_i) = \frac{1}{\hbar}\int_0^T \left(V(Y_i + y_i) + \frac{1}{2} g n_0(y_i) + g n_0(Y_i - Y_j + y_i) \right) dt. \tag{3}$$

The reduction in the atomic density due to splitting has been included explicitly.

To evaluate (3), we require the $Y_i(t)$. If the condensate initially has no motional excitation, then $Y_1(t)=-Y_2(t)$ and we define $Y(t)\equiv Y_1(t)$. (Nonzero initial motion could be incorporated, but in our experiment it is small enough to neglect.) After splitting at $t=0$, the trajectory is initially described by

$$Y(t) = \frac{v_0}{\omega}\sin(\omega t) \quad (t < \tau). \tag{4}$$

The reflection pulse at time τ provides a velocity kick of $-2v_0$, so the subsequent trajectory is

$$Y(t) = \frac{v_0}{\omega}\{\sin(\omega t) - 2\sin[\omega(t-\tau)]\} \quad (\tau < t < 2\tau). \tag{5}$$

Note that the reflection pulse provides a fixed momentum kick and not a true reflection. This introduces asymmetry to the motion, since the packet speed during the second one-half of the trajectory is greater than that during the first. At the recombination time $T=2\tau$, the speed has increased to $v_0(2\cos\omega\tau-\cos 2\omega\tau)$, or approximately $v_0(1+\omega^2\tau^2)$ for $\omega\tau \ll 1$. Also, the two packets are not perfectly overlapped at recombination [14], since $Y(T)\approx -v_0\omega^2\tau^3 \neq 0$. These effects are small for our conditions. For instance, at $\tau=10$ ms, the velocity shift is $5\times10^{-3}v_0$ and the packet displacement is approximately $10^{-2}L$. The displacement could be corrected by shortening the duration of the second part of the trajectory by about 60 μs, but we observe no effect for such small adjustments in the experiment. We therefore use equal times for simplicity.

In principle, the trajectory will also be modified by interactions between the packets. The potential energy of one packet due to the other is

$$U(Y) = \frac{g}{2}\int n_0(y-Y)n_0(y+Y)dy, \tag{6}$$

which has a maximum

$$U(0) = \frac{8}{15}\frac{\mu^2 L}{g} = \frac{2}{5}\mu N. \tag{7}$$

where $N\approx 10^4$ is the number of atoms in the initial condensate. The net interaction energy per atom is thus $U(0)/(N/2)\approx 2\pi\hbar\times 6$ Hz, while the initial kinetic energy is $E_0=mv_0^2/2\approx 2\pi\hbar\times 15$ kHz. The change in velocity due to the interaction between packets is thus only $2\times10^{-4}v_0$, making the effect on the trajectory negligible.

Three terms contribute to the phase: The confinement potential, the self-interaction energy, and the intrapacket interaction energy. The phase of packet 1 due to the confining potential is

$$\phi_1^c(y) = \frac{1}{\hbar}\int_0^T V(y_1 + Y(t))dt. \tag{8}$$

Since y_1 is constant, the final position y relative to the trap center is given by $y=y(T)=y_1+Y(T)$, so

$$\phi_1^c(y) = \frac{1}{\hbar}\int_0^T V(y - Y_f + Y(t))dt, \tag{9}$$

where $Y_f\equiv Y(T)\approx -v_0\omega^2\tau^3$. A similar expression hold for the phase of packet 2, but with $y_2=y+Y_f$. The phase difference is thus

$$\phi^c(y) = \frac{m\omega^2}{2\hbar}\int_0^T [y - Y_f + Y(t)]^2 - [y + Y_f - Y(t)]^2 dt \tag{10}$$

$$= \frac{2m\omega^2}{\hbar} y\left(\int_0^T Y(t)dt - TY_f\right). \tag{11}$$

Evaluation yields

$$\phi^c(y) = -4ky[1 - 2\cos\omega\tau + \cos 2\omega\tau + (2\omega\tau\sin 2\omega\tau - 4\omega\tau\sin\omega\tau)], \tag{12}$$

where we used $v_0=2\hbar k/m$. For $\omega\tau\ll 1$, $\phi\rightarrow 4ky(\omega\tau)^2$, which gives a gradient $d\phi^c/dy$ of 8.5 rad/L at $\tau=10$ ms. The correction due to nonzero Y_f is given by the final two terms in (12), which reduce to $-8ky(\omega\tau)^4$ and are thus negligible.

The phase due to the packets' self-interactions is

$$\phi^s(y) = \frac{g}{2\hbar}\int_0^T n_0(y_1) - n_0(y_2)dt \tag{13}$$

$$= \frac{gT}{2\hbar}[n_0(y - Y_f) - n_0(y + Y_f)] \tag{14}$$

$$= \frac{m\omega^2}{\hbar} yTY_f, \tag{15}$$

where we used $2\mu=m\omega^2L^2$ in the last line. As above, this

effect is of order $(\omega\tau)^4$ and is thus negligible.

The phase on packet 1 due to interactions with packet 2 is

$$\phi_1^i(y) = \frac{g}{\hbar}\int_0^{2\tau} n_0(y + 2Y - Y_f)dt. \tag{16}$$

The piecewise nature of the integrand makes this term complicated. To estimate it analytically, we make several approximations. First, we neglect the small correction Y_f. Second, we take the packet velocity as constant during the time in which the packets are overlapped. This is reasonable since the packet separation time is $t_s = L/v_0 = 4.6$ ms, so the velocity variation $(1/2)(\omega t_s)^2 v_0$ is only $5\times10^{-4}v_0$. Third, we ignore the small change in velocity between the outgoing and returning trajectories. All of these effects can be shown to contribute to the phase at order $(\omega\tau)^4$ or higher.

What remains is

$$\phi_1^i(y) = \frac{2\mu}{\hbar}\int_0^{\min(t_1,\tau)} \left(1 - \frac{(y + 2v_0 t)^2}{L^2}\right)dt \tag{17}$$

for separation time

$$t_1(y) = \frac{L}{2v_0}\left(1 - \frac{y}{L}\right). \tag{18}$$

Packet 2 experiences a similar effect, but with $y + 2v_0 t \to y - 2v_0 t$ in the integral and with a different separation time

$$t_2(y) = \frac{L}{2v_0}\left(1 + \frac{y}{L}\right). \tag{19}$$

Evaluating these integrals yields a differential phase

$$\phi^i(y) = \frac{2\mu}{\hbar}\left[(t_A - t_B)\left(1 - \frac{y^2}{L^2}\right) - 2\frac{(t_A^2 + t_B^2)v_0}{L^2}\left(\frac{2}{3}v_0(t_A - t_B) + y\right)\right] \tag{20}$$

for $t_A(y) = \min(t_1, \tau)$ and $t_B(y) = \min(t_2, \tau)$. This varies with y in a complicated way, but evaluated at $y = 0$ it gives

$$\left.\frac{d\phi^i}{dy}\right|_{y=0} = -8k(\omega t_A)^2, \tag{21}$$

where here $t_A = t_B = \min(\tau, L/2v_0)$. The gradient varies quadratically with $\omega\tau$ like the confinement effect ϕ^c, but only for short times. In our case, $d\phi^i/dy|_{\tau=t_s/2} = -1.1$ rad$/L$, which is small but not negligible. In comparison to Eq. (12), we see that ϕ^c becomes the dominant contribution for experiments in which $\tau > t_s$ such that the packets are well separated.

After recombination, the fraction of atoms brought to rest is ideally $N_0/N = \cos^2[(\theta + \phi)/2]$, where θ is an applied phase and ϕ is the total phase calculated above. Since ϕ depends on position, the final packet density will exhibit a sinusoidal modulation. This can be experimentally observed: The recombination pulse produces three packets, at velocities of 0, v_0, and $-v_0$. After the pulse, we wait some time for these packets to separate and then use a resonant probe beam to take an absorption image. Figure 2 shows examples of the images obtained. Image (a) shows the initial condensate, with no gradient. Images (b) and (c) show packets obtained after the interferometer sequence that exhibit clear spatial modulation.

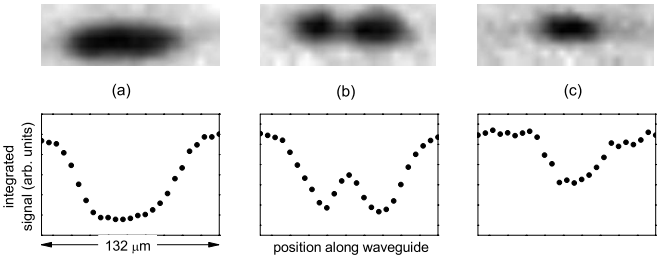

FIG. 2. Absorption images of wave packets used in the condensate interferometer. (a) The condensate distribution, before the interferometer operation. (b), (c) Packets observed in the interferometer output, for two different phase offsets θ. The graphs show the absorption signals integrated along the transverse direction, which are analyzed to determine the modulation period and thereby the phase gradient.

To analyze such images, we integrate the absorption signal in the direction transverse to the interferometer axis, thereby obtaining a one-dimensional profile as seen in the figure. We simultaneously fit profiles of several packets to a modulated Thomas-Fermi function with a common gradient G and fixed width L

$$A(y) = A_0 + B\cos[\theta + Gy]\min\left[0, 1 - \left(\frac{y - y_0}{L}\right)^2\right]. \tag{22}$$

Each of the images in a set is taken with the same experimental conditions except for the applied phase θ, which is varied. From the fit, we acquire $G = |d\phi/dy|$.

Figure 3 shows the measured gradients as functions of the total measurement time $T = 2\tau$. The solid line shows the calculated gradient evaluated at $y = 0$. The measurements agree well with the theoretical prediction.

Since different parts of the packets recombine with different phases, the overall visibility of the interference signal is reduced. The total number of atoms brought to rest is given by

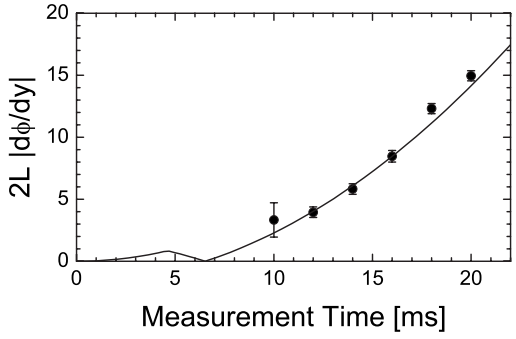

FIG. 3. Magnitude of the phase gradient for a single-sided interferometer of total duration $2\tau_1$. Points show the experimental measurements, with error bars determined by the fitting procedure. The curve shows the results of the calculation described in the text, with the gradient scaled to the length of the packet, $2L$.

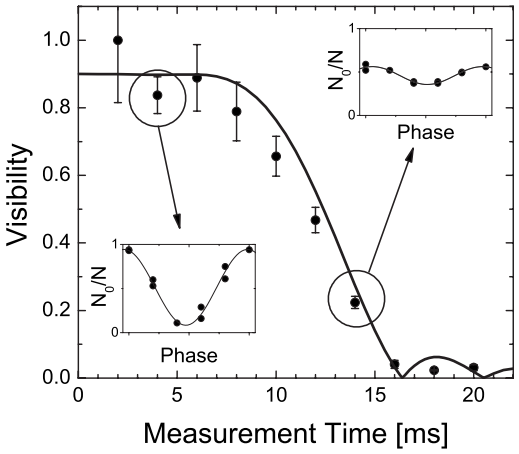

FIG. 4. Visibility of the single-sided interferometer, as a function of total duration. Points show the measured values, while the curves show the theoretical estimation using the rigid packet model. The prediction has been scaled by 0.9 to account for experimental imperfections that are expected to be independent of duration. The insets show example interference curves at the points indicated.

$$N_0 = \frac{1}{2}\left(N + \int n_0(y)\cos[\theta + \phi(y)]dy\right), \tag{23}$$

where the imperfect overlap of the final wave packets is neglected. This yields an interference visibility

$$V = \frac{1}{N}\int n_0(y)\cos\,\phi(y)dy. \tag{24}$$

Experimentally, the visibility and its uncertainty are measured by scanning θ and fitting the resulting signal to the form $(1+V\cos\,\theta)/2$. Figure 4 shows a comparison of the measured and predicted visibility curves. At short times, we obtain typical visibilities of about 0.9, due to imperfections in the standing wave operations, imaging, fitting, and other time-independent experimental limitations. We therefore scale the theoretical curve by this factor. Again, good agreement is obtained, definitively showing that the phase gradient effect is the limiting factor for the interferometer performance.

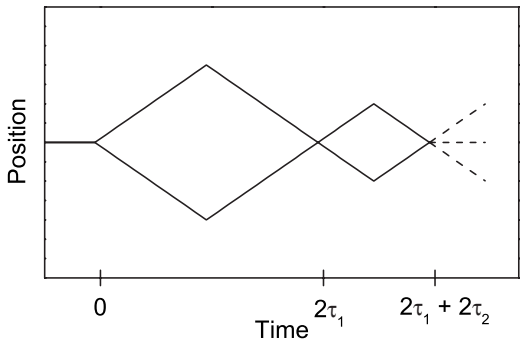

FIG. 5. Packet trajectories for the double-sided interferometer configuration. The packets are split at time $t=0$, reflected at time τ_1, reflected again at time $2\tau_1+\tau_2$, and finally recombined at time $2\tau_1+2\tau_2$. For a symmetric interferometer with $\tau_1=\tau_2$, the phase gradients on the packets are nearly eliminated.

The visibility is reduced by one-half at $T\approx 12$ ms, corresponding to a gradient of 4 radians across the full packet. At this time, the centers of the clouds are 120 μm apart and the packets are just separated. This makes it difficult, for instance, to apply a field to one packet without influencing the other.

It is possible to operate the interferometer with larger phase gradients, by considering the density profile as above and taking the fit phase θ in Eq. (22) as the interferometer output. However, this introduces considerable noise in practice because of imaging limitations such as the imperfect spatial resolution.

III. DOUBLE-SIDED INTERFEROMETER

It is evident from the above discussion that the dominant contribution to the phase gradient comes from the $\int Ydt$ term in ϕ^c, Eq. (12). This explains why the gradient can be reduced by using a trajectory in which Y alternates sign so that $\int Ydt$ is close to zero. One such approach is the double-sided interferometer shown in Fig. 5. We consider an asymmetric interferometer with leg duration τ_1 in the first one-half and τ_2 in the second one-half. The packet trajectory is given by

$$Y(t) = \frac{v_0}{\omega}\begin{cases} \sin\,\omega t & (t<\tau_1), \\ \sin\,\omega t - 2\,\sin\,\omega(t-\tau_1) & (\tau_1<t<2\tau_1+\tau_2), \\ \sin\,\omega t - 2\,\sin\,\omega(t-\tau_1) + 2\,\sin\,\omega(t-2\tau_1-\tau_2) & (t>2\tau_1+\tau_2). \end{cases} \tag{25}$$

Again, the effects of interactions on the trajectory are neglected.

The calculation of ϕ^c and ϕ^s can be performed just as for the single-sided case, yielding

$$\phi^c = 4ky\{1-2\cos u_2 + 2\cos(u_1+2u_2) - \cos(2u_1+2u_2) - 2(u_1+u_2)[\sin 2(u_1+u_2) - 2\sin(u_1+2u_2) + 2\sin u_1]\} \tag{26}$$

and

$$\phi^s = 4ky(u_1+u_2)[\sin 2(u_1+u_2) - 2\sin(u_1+2u_2) + 2\sin u_1] \tag{27}$$

for $u_i = \omega\tau_i$.

The intrapacket effect is again complicated, and because the phase cancels to lowest order, the simplifying approximations used in the single-sided case are not permissible. We can, however, calculate analytically the phase gradient $d\phi^i/dy$ evaluated at $y=0$. From (16),

$$\frac{d\phi_1^i}{dy} = \frac{g}{\hbar}\int_0^T \left.\frac{dn_0}{dy}\right|_{2Y-Y_f} dt = -\frac{2\mu}{\hbar L^2}\int_C 2Y - Y_f dt, \tag{28}$$

where the integral is over times when the packets are overlapped, given by $n_0(2Y-Y_f)>0$. The gradient in packet 2 is equal and opposite to this, making the total phase gradient

$$\frac{d\phi^i}{dy} = -\frac{2m\omega^2}{\hbar}\int_C 2Y - Y_f dt. \tag{29}$$

Evaluation for the trajectory of (25) yields

$$\frac{d\phi^i}{dy} = k(\omega t_s)^2\left[(u_1^2-u_2^2)\left(1-u_1u_2-\frac{7}{12}(u_1^2+u_2^2)\right) - u_1u_2(u_1+u_2)^2\right] \tag{30}$$

to order ω^6. As before, $t_s = L/v_0$ is the packet separation time, and we have assumed $\tau_1, \tau_2 > t_s/2$. If $\tau_1 > t_s/2$ and $\tau_2 < t_s/2$, then the gradient reduces to

$$\frac{d\phi^i}{dy} = -2k\omega^2(t_s^2 - 4\tau_2^2) \tag{31}$$

to leading order.

We performed an experiment in which we fixed $\tau_1 = 10$ ms and varied τ_2. In general, we observed modulation in the output packets as in Fig. 2, from which we obtain an estimated gradient by fitting to Eq. (22). The results are shown in Fig. 6(a). The solid curve shows the total predicted gradient $d\phi/dy$ at $y=0$. It is seen that when $\tau_1 = \tau_2$, the gradient largely cancels, as expected. Figure 6(b) shows how the resulting visibility is recovered. We note that the cancellation effect is very much analogous to the spin echo-phenomenon known in magnetic resonance studies.

With a symmetric interferometer $\tau_1 = \tau_2 \equiv \tau$, the measurement time can be significantly extended compared to a single-sided interferometer, as seen in Fig. 7. The total measurement time T is increased by a factor of 6, while τ and the packet separation are increased by a factor of 3. The separation distance of 0.4 mm is now substantially greater than the packet size.

In the symmetric case, the theoretical value of the phase is, to leading order,

$$\phi = -\tfrac{64}{3}ky(\omega\tau)^6. \tag{32}$$

The predicted visibility is shown as the solid curve in Fig. 7 and is seen to extend to considerably longer times than experimentally observed. However, at such long times, the assumption that $\omega T \ll 1$ no longer holds, meaning that the rigid-packet model is not justified. Stickney *et al.* have analyzed the case of a symmetric double-sided interferometer using a model in which variation of the packet length is included to lowest order [15]. They find a leading-order phase of

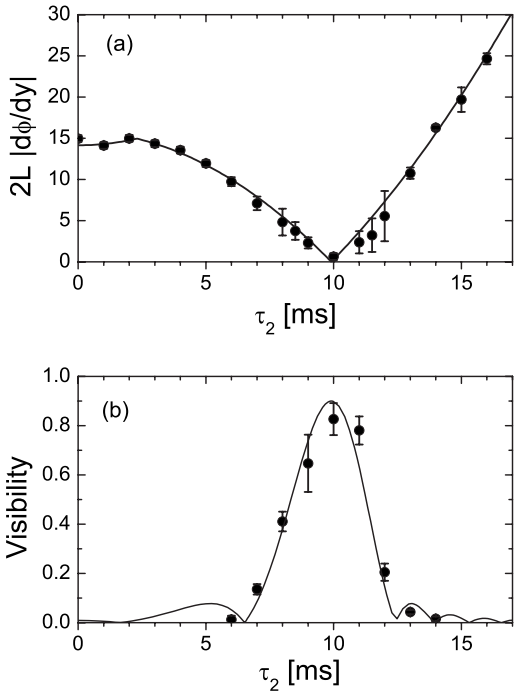

FIG. 6. (a) Phase gradient observed in an asymmetric double-sided interferometer. The first one-half of the trajectory used leg time $\tau_1 = 10$ ms and the second one-half used τ_2. When $\tau_2 = \tau_1$, the phase gradient is nearly eliminated. (b) Interferometer visibility as τ_2 is varied. For both plots, data points show the experimental results and the curves show the model calculation. The calculation in (b) is scaled by 0.9 to account for time-independent imperfections as in Fig. 4.

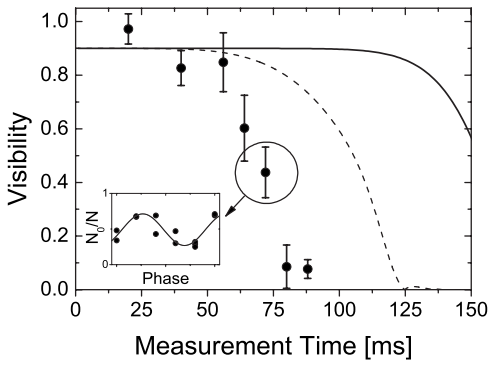

FIG. 7. Visibility of the symmetric double-sided interferometer, as a function of the total measurement time $T = 4\tau$. Data points show the experimental results and the curves show the predictions of the rigid-packet model (solid) and a dynamic packet model (dashed) [15], each scaled by 0.9 as in Fig. 4. The inset shows an example interference curve at $T = 72$ ms.

$$\phi = -88ky(\omega\tau)^6, \tag{33}$$

resulting in the dashed curve in Fig. 7. This is in better agreement with the experiment, though it still predicts a larger coherence time than observed.

A possible reason for the discrepancy is that the model is one dimensional. The experiment is not in the one-dimensional regime, so packet dynamics will occur in the transverse directions as well. Since the different directions are coupled by the interactions, the dynamics in the y direction will have components at the transverse frequencies [16], which could be significant and non-rivial on the time scales observed here.

In the experiment, images of the atoms do not exhibit gradients like those seen in Fig. 2 as the visibility of the double-sided interferometer falls to zero. Instead, the recombination appears to be uniform. This might also be explained by transverse dynamics, if a transverse gradient develops along with the longitudinal one. This would mask the longitudinal gradient, since the absorption imaging technique averages over phase variations that are parallel to the probe beam. Such gradients are possible if the standing-wave laser axis is not aligned precisely to the principle axis of the guide potential.

Some other reasons for the decay of the visibility can be ruled out. For instance, we verified that the two packets are spatially overlapped at recombination by imaging the packets from two different directions. Also, overall phase noise such as that resulting from vibrations of the mirror producing the standing wave would cause the interferometer signal to vary and reduce the visibility upon averaging. However, we do not observe the shot-to-shot fluctuations that would characterize such noise. For instance, at a total measurement time $T=100$ ms, the deviation in N_0/N from one experiment to the next is only 1%.

IV. FREE-OSCILLATION INTERFEROMETER

The double-sided interferometer is more symmetric than the single-sided one, but the velocity errors imposed by the reflection pulses prevent it from being perfectly symmetric. More accurate phase cancellation can be obtained if the reflection pulses are avoided all together, and the atoms instead allowed to complete a full natural oscillation in the guide, as in Fig. 8. Insofar as the guide potential is harmonic, the trajectories for the two half-cycles will be balanced and any phase gradients should cancel precisely. Even if the packets evolve in a complicated way, the evolution should be symmetric and thus any resulting phases should cancel.

However, over the oscillation period of 0.9 s, many external noise sources can impart an uncontrolled phase difference to the packets, making the interferometer output effectively random. We were therefore unable to observe a controlled interference signal as in the previous experiments, but rather used the run-to-run variations in the output as a measure of the interference visibility. The presence of large fluctuations indicates that interference is occurring, while an unvarying output indicates the visibility of the interference is zero

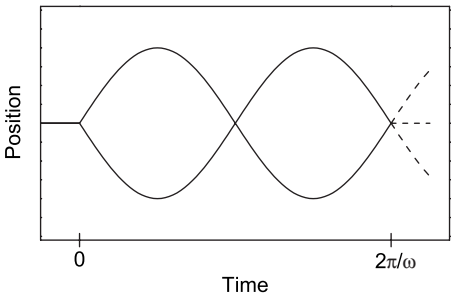

FIG. 8. Packet trajectories for the free-oscillation interferometer. The packets are split at time $t=0$ and then complete a full oscillation in the harmonic guide potential before being recombined. Here ω is the oscillation frequency in the guide.

To obtain long measurement times, the standing wave beam must be well aligned to the guide axis, to avoid having the packets miss each other in the transverse directions. In Fig. 9, we show the variance of N_0/N observed as the beam angle is varied, plotted against the measured packet displacement. The clear peak indicates that interference is present. Assuming the fluctuations represent an underlying distribution $(1+V\cos\theta)/2$ with random θ, the variance Δ^2 is related to the visibility V by $\Delta^2=V^2/8$, thus suggesting $V=0.3$. We note that no fluctuations were observed when the atoms were allowed to oscillate for only one-half of the axial period.

The technique of using a freely oscillating trajectory was also recently demonstrated by Segal *et al.* [17] and by Horikoshi and Nakagawa [9]. In both cases, fluctuations similar to ours were observed at the longest interferometer times. Horikoshi and Nakagawa were also able to operate their experiment at a higher ω and achieve a stable output phase, which supports the hypothesis that the fluctuations are an effect of low-frequency external noise, such as vibrations of the table on which the experiment is mounted.

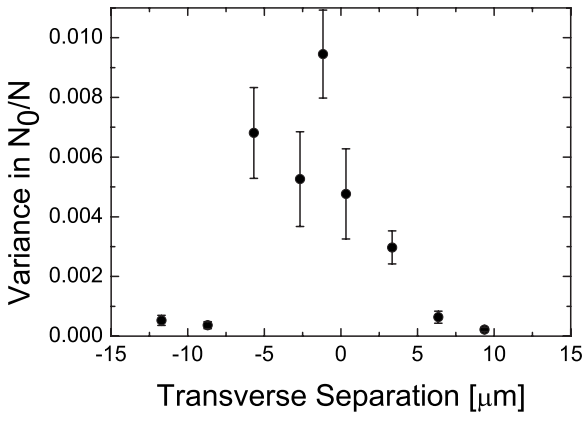

FIG. 9. Interference for atoms freely oscillating in the waveguide. The measurement time is 0.9 s, corresponding to a separation of 1.7 mm. The phase of the interference is random, so the variance of the signal measured over several experiments is plotted against the transverse separation of the wave packets at the time of the recombination pulse. The large increase in variance when the packets are overlapped is taken as a signal that interference is present. The error bars represent the error in the variance, estimated as Δ^2/N for variance Δ^2 and number of measurements N.

Without control of the overall phase, it is not possible to make use of our results in a practical measurement. However, it seems likely that this is a technical problem that is solvable through various stabilization methods. If so, this type of interferometer would offer an unprecedented arm separation and measurement time.

V. CONCLUSIONS

We have studied the effect of longitudinal confinement on a guided-wave atom interferometer, under various conditions. It is seen conclusively that for a single-sided interferometer, large phase gradients induced by the confinement potential place a severe limit on the usable arm separation of the interferometer. The phase gradients were measured and found to agree well with a simple theory in which the internal dynamics of the atomic wave packets are neglected.

The interferometer performance can be significantly improved using a double-sided trajectory, in which each packet experiences each side of the potential. In this case, measurement times of up to 72 ms and arm separations of 420 μm are achieved. An even larger arm separation of 1.7 mm can be obtained by allowing the packets to complete a full oscillation in the guide, with no imposed reflection pulses. In this case, however, noise effects introduce a random phase shift that prevents the device from being practically useful. When the measurement time of the interferometer becomes comparable to the motional period in the transverse directions of the guide, accurate predictions of performance will likely require a more sophisticated model in which the transverse dynamics are included.

To put these results in context, one can define a figure of merit χ for an atom interferometer as the time integral of the wave-packet separation. This is proportional to the accumulated phase for measurement of a linear gradient field such as gravity, and for a given atom velocity, it is also proportional to the Sagnac phase in a loop geometry. Previous results for our experiment were limited to $\chi=6$ μm s [6], and other approaches have yielded $\chi\lesssim 4$ μm s [8,9,18] with controlled phase and $\chi=66$ μm s with uncontrolled phase [17]. The improvements reported here give $\chi=15$ μm s with controlled phase and 1600 μm s with uncontrolled phase. In comparison, free space interferometers reach $\chi\approx 500$ μm s with a controlled phase [19,20].

We do note that symmetric interferometers of the type presented here are not suited for some types of measurements. In a measurement of gravity, for instance, the gravitational phase of the two arms would cancel just as the confinement phase does. However, many other measurements remain possible, including the Sagnac phase in a loop geometry and any case where the effect to be measured can be applied at a definite time. We have recently used this technique to interferometrically measure the dynamic polarizability of ^{87}Rb [21].

A natural conclusion to be drawn is that axial confinement in a guided-wave interferometer is generally a detriment and should be avoided. In a linear interferometer such as the one described here, the axial field variation is mostly produced by the electrical connections at the end of the guide. In this case, simply making the guide longer would improve the flatness by moving the connections further away [5]. Alternatively, additional current elements could be added to flatten the potential in the center of the guide.

It may also be noted that gradient effects would generally be suppressed in a ring-shaped guide. Even if the potential around the ring is not uniform, the net phase gradient will be close to zero if the packets are allowed to propagate around the full circumference. The lack of reflection pulses makes this case similar to the free-oscillation interferometer demonstrated here. Through considerations such as these, we expect that the findings here will be useful for guiding future designs.

ACKNOWLEDGMENTS

We are grateful to J. Stickney, A. Zozulya, and D. Anderson for useful conversations on these subjects. This work was funded by the U.S. Defense Advanced Research Projects Agency and Army Research Office, under Grant No. W911NF-06-1-0474.

[1] *Atom Interferometry*, edited by P. R. Berman (Academic, San Diego, 1997).
[2] Y. Shin, M. Saba, T. A. Pasquini, W. Ketterle, D. E. Pritchard, and A. E. Leanhardt, Phys. Rev. Lett. **92**, 050405 (2004).
[3] T. Schumm, S. Hofferberth, L. M. Anderssona, S. Wildermuth, S. Groth, I. Bar-Joseph, J. Schmiedmayer, and P. Krüger, Nat. Phys. **1**, 57 (2005).
[4] Y. J. Wang, D. Z. Anderson, V. M. Bright, E. A. Cornell, Q. Diot, T. Kishimoto, M. Prentiss, R. A. Saravanan, S. R. Segal, and S. Wu, Phys. Rev. Lett. **94**, 090405 (2005).
[5] S. Wu, E. J. Su, and M. Prentiss, Eur. Phys. J. D **35**, 111 (2005).
[6] O. Garcia, B. Deissler, K. J. Hughes, J. M. Reeves, and C. A. Sackett, Phys. Rev. A **74**, 031601(R) (2006).
[7] M. Horikoshi and K. Nakagawa, Phys. Rev. A **74**, 031602(R) (2006).
[8] G.-B. Jo, Y. Shin, S. Will, T. A. Pasquini, M. Saba, W. Ketterle, D. E. Pritchard, M. Vengalattore, and M. Prentiss, Phys. Rev. Lett. **98**, 030407 (2007).
[9] M. Horikoshi and K. Nakagawa, Phys. Rev. Lett. **99**, 180401 (2007).
[10] J. M. Reeves, O. Garcia, B. Deissler, K. L. Baranowski, K. J. Hughes, and C. A. Sackett, Phys. Rev. A **72**, 051605(R) (2005).
[11] S. Wu, Y. Wang, Q. Diot, and M. Prentiss, Phys. Rev. A **71**, 043602 (2005).
[12] K. J. Hughes, B. Deissler, J. H. T. Burke, and C. A. Sackett, Phys. Rev. A **76**, 035601 (2007).
[13] M. Olshanii and V. Dunjko, e-print arXiv:cond-mat/0505358.
[14] J. A. Stickney, D. Z. Anderson, and A. A. Zozulya, Phys. Rev.

A **75**, 063603 (2007).
[15] J. A. Stickney, R. P. Kafle, D. Z. Anderson, and A. A. Zozulya, Phys. Rev. A **77**, 043604 (2008).
[16] F. Dalfovo, S. Giorgini, L. Pitaevskii, and S. Stringari, Rev. Mod. Phys. **71**, 463 (1999).
[17] S. R. Segal, Q. Diot, E. A. Cornell, M. Prentiss, A. A. Zozulya, and D. Z. Anderson, Bull. Am. Phys. Soc. **52**, 11 (2007).
[18] E. Su, S. Wu, and M. Prentiss, e-print arXiv:physics/0701018.
[19] A. Peters, K. Y. Chung, and S. Chu, Metrologia **38**, 25 (2001).
[20] J. M. McGuirk, G. T. Foster, J. B. Fixler, M. J. Snadden, and M. A. Kasevich, Phys. Rev. A **65**, 033608 (2002).
[21] B. Deissler, K. J. Hughes, J. H. T. Burke, and C. A. Sackett, Phys. Rev. A **77**, 031604(R) (2008).